Phase separation and stability in $Sm_{0.50}Sr_{0.50}MnO_3$: effects of cation dopants

2008 J. Phys.: Condens. Matter 20 075221

(http://iopscience.iop.org/0953-8984/20/7/075221)

J. Phys.: Condens. Matter **20** (2008) 075221 (12pp) doi:10.1088/0953-8984/20/7/075221

Phase separation and stability in $Sm_{0.50}Sr_{0.50}MnO_3$: effects of cation dopants

Affia Aslam[1], S K Hasanain[1], G Hassnain Jaffari[1], Munib Asim[2], S Ali[3], P Granitzer[4], H Krenn[4], P Knoll[4] and W Lang[5]

[1] Physics Department, Quaid-i-Azam University, Islamabad, Pakistan
[2] A Q Khan Research Laboratories, Islamabad, Pakistan
[3] Government College University, Lahore, Pakistan
[4] Institute of Physics, University of Graz, Austria
[5] Institute of Materials Physics, University of Vienna, Austria

Received 8 October 2007, in final form 31 December 2007
Published 31 January 2008
Online at stacks.iop.org/JPhysCM/20/075221

Abstract

The $Sm_{0.50}Sr_{0.50}MnO_3$ system has been studied with respect to identifying the various electronic and magnetic phases and the effects of introducing different cation dopants on these phases and their respective stabilities. Magnetic, resistive and thermoelectric studies have been performed as a function of temperature in $Sm_{0.50}Sr_{0.50}MnO_3$, $(Sm_{0.50}Nd_{0.50})_{0.50}Sr_{0.50}MnO_3$ and $Sm_{0.50}(Sr_{0.50}Ca_{0.50})_{0.50}MnO_3$. The parent compound ($Sm_{0.50}Sr_{0.50}MnO_3$) lies close to the ferromagnetic–antiferromagnetic (FM–AFM) phase boundary and the consequent effects of the dopants are explained in terms of the changes in the one electron bandwidth and the cation size variation and disorder. Below 130 K the ground state for $Sm_{0.50}Sr_{0.50}MnO_3$ composition is seen to be a mixture of ferromagnetic and A-type antiferromagnetic phases. Partial substitution of a *larger* size cation (Nd) in place of Sm raises the ferromagnetic transition temperature while at the same time stabilizing the AFM phase. This latter trend is inferred from the differences in the hysteresis behaviour of the two systems and is explained in terms of the decrease of the size mismatch factor between cations. However, partial substitution of the *smaller* size cation (Ca) in place of Sr almost eliminates the ferromagnetic phase, leaving the system in a charge ordered state, which appears to be accompanied by the CE type of charge–orbital ordering, exhibiting extremely large values of resistivity.

1. Introduction

Mixed valent manganite perovskites have the generic formula $RE_{1-x}M_xMnO_3$, with RE typically a trivalent rare earth, while M is a divalent alkaline earth. With variation in the divalent to trivalent ion ratio the system assumes a whole range of diverse and often subtle variations of the electronic properties. These include, alongside the metallic to insulating and ferromagnetic to antiferromagnetic transitions, other effects such as charge and orbital ordering, and phase separation on different mesoscopic and sub-mesoscopic levels [1, 2]. A particularly sensitive composition is the so-called 50–50 composition ($x = 0.5$). Here slight variations in x (that affect the ratio of divalent to trivalent ions) or in the average sizes of the trivalent and divalent cations can also cause major changes in the stability of the various phases, as the system moves across various close lying boundaries in the system phase diagram. Thus, even for a fixed value of x, magnetic and transport properties of these materials can be drastically modified by changing the combination of the A-site ions (i.e. RE and M). Not only are the relative stabilities of the various electronic phases affected but also their ability to coexist in a phase separated state. At the atomic level such variations in the properties occur as different combinations of RE and M cause changes in the average cationic radius $\langle r_A \rangle$ [3–5]. For example, as $\langle r_A \rangle$ decreases, the Mn–O–Mn angle further deviates from 180°, hence weakening the ferromagnetic double exchange and reducing the effective one electron bandwidth. This size effect would therefore manifest itself in lowering of the metallicity and ferromagnetic transition.

Another important parameter which is affected by the different combinations of RE and M is the so-called size

mismatch factor for the cations or the variance in the cation size defined as $\sigma^2 = \Sigma y_i r_i^2 - \langle r_A \rangle^2$ [6]. The disorder induced by the mismatch between the cationic sizes strongly affects the various phases that are characterized by different degrees of electron–lattice coupling. Interestingly, Monte Carlo simulations show [7] that, while the random potential introduced by the disorder tends to weaken both the ferromagnetic and the charge ordering (CO) tendencies, the latter (AFM–CO) interactions are suppressed much more strongly because the CO requires a longer range phase coherence to be established than the double exchange. Thus the disorder introduced by size variations can be expected to in general affect the relative stability of the FM and the CO–AFM phases differently.

The commensurate value of the half doped (i.e. $x = 0.50$) composition for these manganites tends to stabilize the charge ordering antiferromagnetic state. However, the subtle balance or competition between ferromagnetic and antiferromagnetic states results in the coexistence of these magnetic phases (e.g. $La_{0.50}Ca_{0.50}MnO_3$) in a narrow range of x and T. Such competition critically depends upon the carrier itinerancy or single electron bandwidth W [3–5], or size mismatch factor between the cations [3, 8, 9], and oxygen stoichiometry [4] etc.

Although the $Sm_{1-x}Sr_xMnO_3$ system corresponds to a larger one electron bandwidth [10] than the $La_{0.5}Ca_{0.5}MnO_3$ ($\langle r_A \rangle$ values varies from 1.132 Å for $x = 0$ to 1.31 Å for $x = 1$), in this system the size mismatch between the cations (σ^2) is much larger, reaching a maximum value of 7.9×10^{-3} Å^2 at $x = 0.5$. According to the phase diagram discussed by Martin *et al* [10], with decrease of temperature the $Sm_{1-x}Sr_xMnO_3$ system undergoes successive transitions from the paramagnetic insulating (PMI) to charge ordered–antiferromagnetic insulating CO–AFMI state and finally from CO–AFMI to FMM for $0.4 \leqslant x \leqslant 0.6$ with low values of the ferromagnetic transition temperature. The extension of the ferromagnetic region of the phase diagram to such large values of x is explained by the existence of the relatively large one electron bandwidth, as discussed above, while the low T_c values observed nonetheless are understood to be due to the larger σ^2 values for the Sm–Sr series.

There is however considerable controversy about the nature and extent of the different phases in this system. Ivanov *et al* [11] have shown that the low temperature phase changes from being ferromagnetic to an A-type antiferromagnetic for x slightly less than 0.5. According to them, the ground state for $Sm_{0.50}Sr_{0.50}MnO_3$ composition for $T < 220$ K is pure AFMI. A similar kind of antiferromagnetic and insulating ground state at low temperatures has been reported by Tomioka *et al* [12] for $Sm_{0.50}Sr_{0.50}MnO_3$ composition.

EPR studies [13] have arrived at a somewhat different conclusion and suggest that for this particular composition ($Sm_{0.50}Sr_{0.50}MnO_3$) some PM domains convert to short range charge ordered (CO) ones below $T_{co} \sim 250$ K and form a mixed or two component state (PM + CO). According to the authors some AFM domains also grow along with the mixed phase below $T_N \sim 170$ K, and finally this three phase system transforms almost completely to the FM phase at $T_c \sim 130$ K with very small traces of AFM phase.

Recent structural investigations using neutron diffraction and electron microscopy [14] have shown that the $Sm_{0.50}Sr_{0.50}MnO_3$ system reveals a phase separated (PS) ground state for $T < 135$ K with coexistence of two structural phases, having the same crystallographic space group but with different sets of unit cell parameters. The authors have explained this PS state by the coexistence of FM and AFM states, which shows metallic-like characteristics below 50 K.

In the background of these reports that clearly illustrate the complex nature of the electronic phases of the $Sm_{0.50}Sr_{0.50}MnO_3$ system, including the indications of two phase coexistence and the suggestions of short range charge order in this system, we have used a variety of measurements including resistivity, magnetization and thermopower to identify and explore the different magnetic phases present and their dependence on temperature, field and thermomagnetic history of the material. While similar work on some aspects of resistivity and magnetization for this particular composition has been already reported by some groups [10–12], to our knowledge thermoelectric power (TEP) measurements for the $Sm_{0.50}Sr_{0.50}MnO_3$ composition have not been reported. As the thermopower has separate contributions arising from the different components (diffusion, phonon, magnetic etc) operative in the different phases, its temperature dependence enables the presence and extent of difference phases to be better identified, as compared to simple transport measurements. We have also studied the effect of cation size changes in this composition as the trivalent Sm is replaced partially by the larger size Nd and, separately, the divalent Sr is partially replaced by the smaller size Ca (i.e. $(Nd_{0.50}Sm_{0.50})_{0.50}Sr_{0.50}MnO_3$ and $Sm_{0.50}$ $(Sr_{0.50}Ca_{0.50})_{0.50}MnO_3$) respectively. Although the doped compositions are expected to have the same hole density as that without doping, i.e. $Sm_{0.50}Sr_{0.50}MnO_3$, different values of the average cationic radius and the size mismatch factor due to the dopants can lead to drastic effects on the magnetic phases present. We shall show how the combination of the average size variation and size mismatch factor operating on the ferromagnetic and CO phases respectively leads to the extension or reduction in the stability of these phases and sometimes to the development of thermomagnetic history dependence of the phases.

2. Experiment

Polycrystalline samples of the compositions $Sm_{0.50}Sr_{0.50}MnO_3$, $(Nd_{0.50}Sm_{0.50})_{0.50}Sr_{0.50}MnO_3$ and $Sm_{0.50}(Sr_{0.50}Ca_{0.50})_{0.50}MnO_3$ were prepared using the solid-state reaction method. Stoichiometric amounts of respective oxides or carbonates (all having 99.9% purity) were thoroughly mixed, ground and initially calcined at 1000 °C for 16 h. The products were reground and re-heated at 1100 °C for 17 h. Following the cool-down, the material was again ground to fine powder and pressed into pellets. Finally, these pellets were heated at 1400 °C for 8 h.

Structural characterization was performed using a JDX-11 x-ray diffractometer with Cu Kα (1.5418 Å) radiation. XRD patterns for all three compositions are shown in figure 1. At room temperature, all three compositions have orthorhombic

Table 1. Lattice parameters of $(Nd_{0.50}Sm_{0.50})_{0.50}Sr_{0.50}MnO_3$, $Sm_{0.50}Sr_{0.5}MnO_3$, and $Sm_{0.50}(Sr_{0.50}Ca_{0.50})_{0.5}MnO_3$ compositions.

Lattice constants (Å)	$(Nd_{0.50}Sm_{0.50})_{0.50}Sr_{0.50}MnO_3$	$Sm_{0.50}Sr_{0.50}MnO_3$	$Sm_{0.50}(Sr_{0.50}Ca_{0.50})_{0.50}MnO_3$
a	5.463	5.447	5.402
b	5.423	5.419	5.405
c	7.624	7.638	7.611

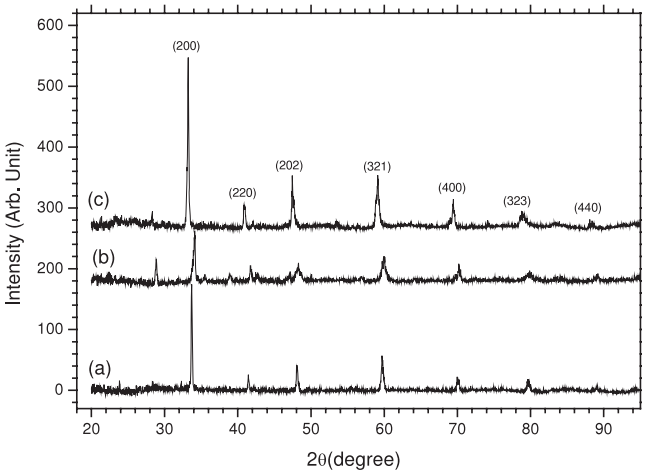

Figure 1. XRD patterns of (a) $Sm_{0.50}$ $(Sr_{0.50}Ca_{0.50})_{0.5}MnO_3$, (b) $Sm_{0.50}Sr_{0.5}MnO_3$ and (c) $(Nd_{0.50}Sm_{0.50})_{0.50}Sr_{0.50}MnO_3$.

unit cell with *Pnma* crystal symmetry. Substitution of Sm by Nd and of Sr by Ca does not yield any phase changes in the parent (undoped) $Sm_{0.50}Sr_{0.5}MnO_3$ composition. One unidentified peak is observed in the undoped and Nd doped compositions at 2θ about 29° that suggests the trace of an impurity. The lattice parameters obtained using the least square fit procedure for these three compositions are given in table 1. These values are comparable to those reported by other authors for the same systems [15]. It is clear that the partial substitution of Sm by a slightly larger sized Nd leads to a slight increase of the a, b lattice parameters while the partial substitution of Sr by the smaller Ca ion decreases all three of the lattice parameters, quite significantly.

The DC resistances were measured from room temperature to 10 K using the standard four probe method. Magnetic measurements were made using a SQUID magnetometer.

TEP measurements were made using a self-made thermoelectric power set-up described in detail elsewhere [16]. All these measurements were made using the differential method with typical temperature gradient of 1–1.5 K between the two ends of the sample. All the data shown were obtained while heating up the sample from the low temperature side, typically from 85 K up to room temperature. Background corrections and reproducibility were carefully checked for all the reported measurements.

3. Results

3.1. Temperature dependence of DC magnetization

Magnetization profiles as a function of temperature (4 K $<$ T $<$ 300 K) were obtained for the $Sm_{0.50}Sr_{0.50}MnO_3$ composition at four different fields (H = 100, 1000, 10 000 and 70 000 Oe) as shown in figure 2. All these data were taken in zero field cooled conditions using a SQUID magnetometer.

At the lowest applied field (100 Oe) the development of different magnetic correlations with the lowering of temperatures can be clearly discerned. Starting from the higher temperature region we consider the data shown in the inset of figure 2 that shows the temperature region from 220 to 130 K on an expanded scale. While not noticeable in the main figure, we observe a small and rather broad peak in the moment around T = 180 K. The same feature was also discernible in the magnetization data at H = 1 kOe and 10 kOe but not at 70 kOe. The high temperature behaviour is analysed by

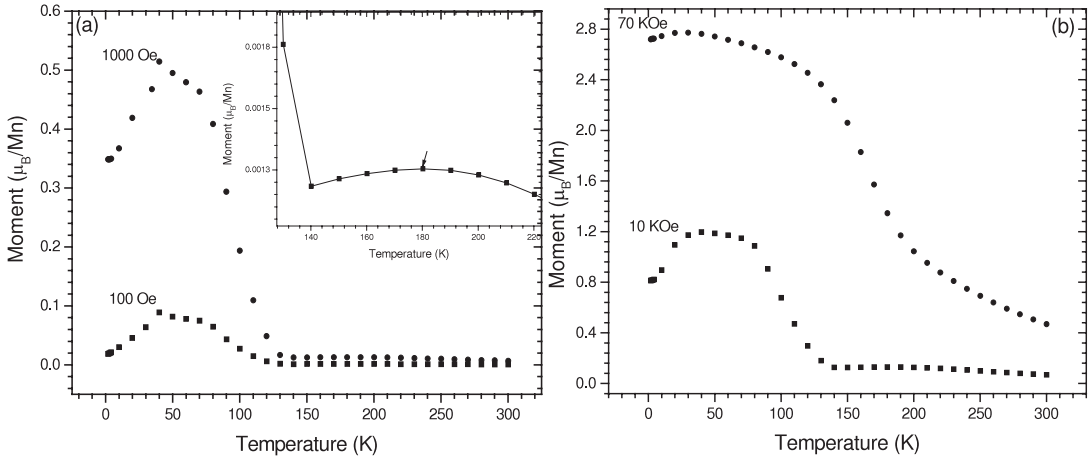

Figure 2. Temperature versus magnetization profiles for $Sm_{0.50}Sr_{0.50}MnO_3$ recorded at different applied fields. The inset shows the $M(T)$ data for the temperature region from 220 to 130 K at expanded scale for a 100 Oe applied field.

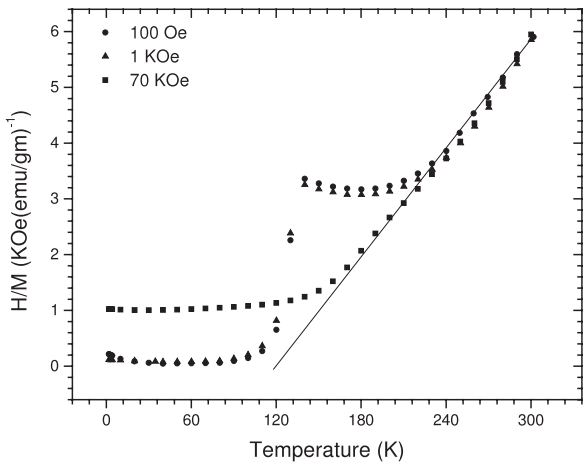

Figure 3. Inverse susceptibility (H/M) versus temperature curves for $Sm_{0.50}Sr_{0.50}MnO_3$; the solid line shows the linear fitting for 100 Oe data.

plotting the inverse susceptibility (H/M) versus temperature in figure 3. From the linearity of the data it is clear that for all the applied fields the system exhibits a Curie–Weiss type behaviour at high temperatures, with the linear variation extrapolating to zero ($\chi \rightarrow \infty$) for $T \sim 120$ K. However, as the temperature is lowered below $T = 230$ K we observe that, except for the 70 kOe magnetization, there is apparently a development of antiferromagnetic correlations as manifest from the positive deviations of the data from the Curie–Weiss behaviour. The development of these AFM correlations is however not very long lived, and at T about 130 K there is a clear transition towards a ferromagnetic state. This is, as expected, a sharp transition for the lower applied fields, while a broad transition is observed for high fields ($H >$ 10 kOe). For the lower applied fields the development of strong antiferromagnetic correlations is clearly manifest in the form of a peak in the magnetization for $T \sim 40$ K. With the application of higher fields, this low temperature AFM phase shifts towards lower temperatures and almost disappears for the 70 kOe applied field. These results for the successive magnetic phases, namely, PM $\rightarrow$ AFM $\rightarrow$ FM, are in agreement with those obtained by Martin *et al* [10] and Damay *et al* [17].

The above behaviour can be summarized by the following sequence. On cooling below 230 K there is the development of antiferromagnetic correlations within the main paramagnetic phase. Further down in the temperature range $T \sim 140$–180 K there is more evidence that an AFM phase has begun to manifest itself, as shown by the slight decrease in the moment. This phase appears to be imbedded within the dominant paramagnetic phase. This suppressed AFM region is followed, for the lower fields, by a clear FM transition for T about 130 K. For very high fields the intermediate AFM region vanishes and the paramagnetic region is followed directly by the ferromagnetic transition.

The above observations can be related to the electron diffraction study [10] for the $Sm_{0.50}Sr_{0.50}MnO_3$ composition, that has shown that at $T \sim 250$ K there is a conversion of part of the homogeneous PM into short range charge ordered (CO) domains. Thus the inhomogeneous state that is suggested by the macroscopic magnetization measurements and their Curie–Weiss plots, for 140 K $< T <$ 230 K, appear to be related to the development of some CO–AFM domains within the predominantly PM phase. The absence of this region at high applied fields clearly indicates the tenuous nature of these CO domains, that cannot be stabilized on the application of high fields.

We now consider the effect of partially substituting Nd for Sm in this system. Figure 4 shows the temperature dependence of the magnetization for the $(Nd_{0.50}Sm_{0.50})_{0.50}Sr_{0.50}MnO_3$ composition. For all the fields there is a major peak in the magnetization for $T \sim 180$–200 K showing FM correlations. However, for fields up to 10 kOe the magnitude of this moment is very small, while it approaches 2.1 μ_B/Mn for $H = 70$ kOe. This would indicate that either the FM alignment is competing with the antiferromagnetic one in this temperature region or that the FM correlations are established in small regions that grow at large fields. For $T < 200$ K there is a sharp decrease in the magnetization consistent with the occurrence of the AFM transition. This AFM transition is arrested at $T \sim 150$ K and below this temperature the system either shows a slight increase or almost constant moment. For low applied fields

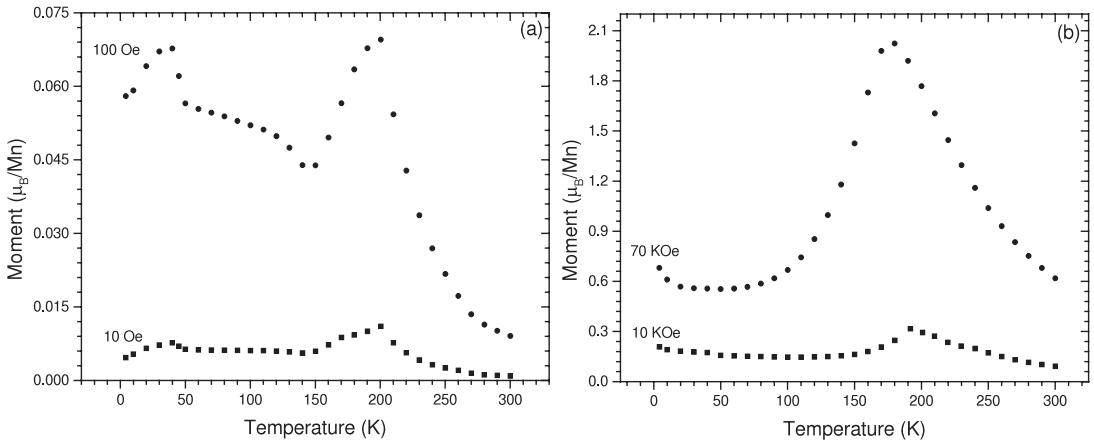

Figure 4. Temperature versus magnetization profiles recorded at different applied fields for $(Nd_{0.50}Sm_{0.50})_{0.50}Sr_{0.50}MnO_3$.

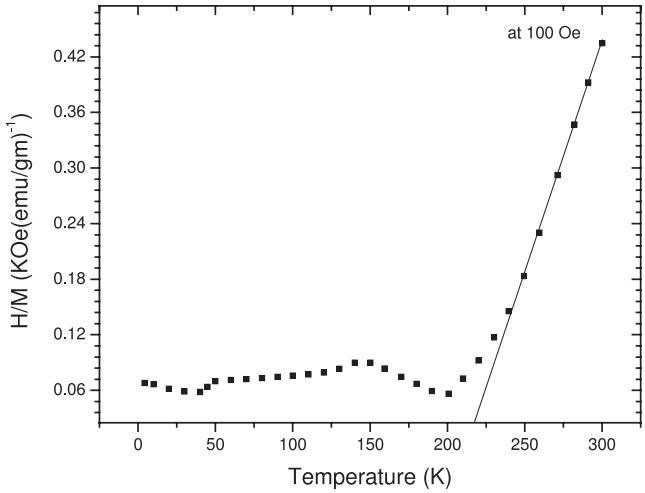

Figure 5. Inverse susceptibility (H/M) versus T curve for $(Nd_{0.50}Sm_{0.50})_{0.50}Sr_{0.50}MnO_3$.

there is also evidence for another antiferromagnetic transition initiating at $T \sim 40$ K. With increasing fields this low temperature AFM transition is pushed to lower temperatures and cannot be evidenced for the highest fields ($H > 10$ kOe). This qualitative description is further strengthened by considering the variation of the inverse susceptibility shown in figure 5. Curie–Weiss behaviour is evident down to 240 K as shown by linear fitting of the H/M versus T curve for a 100 Oe applied field. The data extrapolate to zero at $T \sim 220$ K, suggesting that the FM transition temperature has increased very considerably compared to the pure Sm–Sr system. Due to the limited number of data points in the linear region the actual extrapolated value cannot be taken too seriously; however, the increase compared to the undoped value is definitely a reliable conclusion. The deviation of the data from the extrapolated line in the temperature region 240–200 K again indicates the presence of antiferromagnetic correlations, with the moment increasing more slowly than predicted by the CW law. For $T <$ 200 K the AFM alignment dominates the magnetic response and the moment starts to decrease. As mentioned earlier, for higher fields the antiferromagnetic alignment is shifted towards lower temperatures as the application of high fields tries to stabilize the FM alignment. It appears that *below* 200 K both FM and AFM phases can in general coexist with comparable thermodynamic energies and compete for domination. The relative amounts of the two phases depend on the magnitude of the applied field.

It is also noticeable that even for an applied field of 70 kOe the value of the moment at the FM maximum is about 2 μ_B/Mn, which is significantly less than the expected value of 3.5 μ_B/Mn if all the Mn ions are ferromagnetically aligned in these half doped manganites. Overall these observations show that, even with the addition of Nd, the ferromagnetic correlations have become stronger for $(Nd_{0.50}Sm_{0.50})_{0.50}Sr_{0.50}MnO_3$ composition, resulting in a higher Curie temperature. However, when the maximum value of the moment attained in the highest field is compared for the two compositions (2 as opposed to 2.8), it appears that the overall volume fraction of the FM phase has actually *decreased* in the Nd doped composition as compared to the $Sm_{0.50}Sr_{0.50}MnO_3$ composition. This latter point will be further discussed in the context of the $M(H)$ measurements.

Magnetization and temperature ($M(T)$) data for the Ca doped composition ($Sm_{0.50}(Sr_{0.50}Ca_{0.50})_{0.50}MnO_3$) is shown in figure 6. The system shows a very small fraction of FM alignments present at $T < 110$ K followed by a sharp decline for low applied fields (100 and 1000 Oe). The actual behaviour is however much more complex, as is revealed by the Curie–Weiss plots for the different fields (figure 7). The system shows the Curie–Weiss type linear behaviour down to 230 K. From 230 to 110 K the data show clear deviations from linearity, indicating the presence of AFM correlations. Below 110 K, however, there is an abrupt change in the slope of the H/M versus T variation, suggestive of the growth of FM correlations. This is of course also evident in the sharp rise in the magnetic moment in the same temperature region in figure 6. The low values of the moment (for $H < 70$ kOe) suggest that these FM correlations only exist in small regions, while the marked decline in the moment at 40 K indicates the conversion of these regions into AFM aligned ones. The

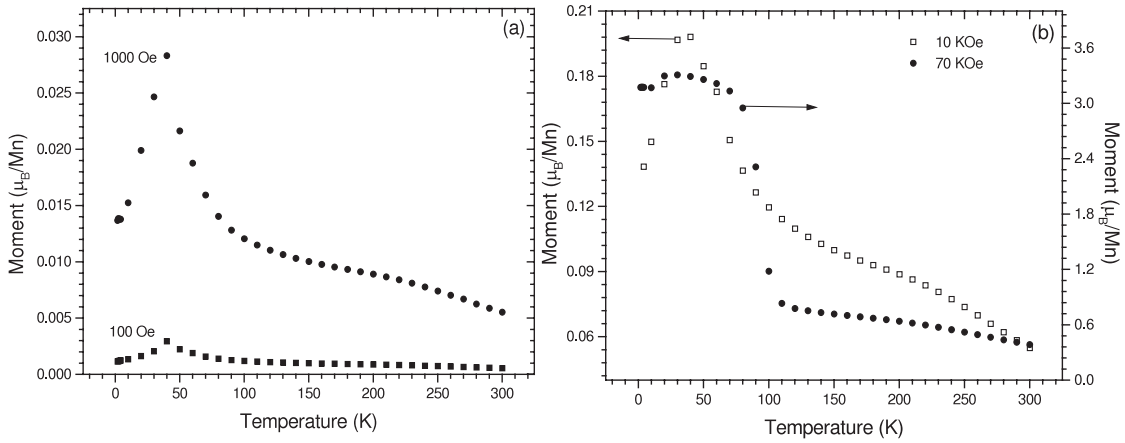

Figure 6. $M(T)$ profiles recorded at different applied fields for $Sm_{0.50}(Sr_{0.50}Ca_{0.50})_{0.50}MnO_3$ composition. In (b) 10 kOe data are shown on the left side Y-axis while 70 kOe data are plotted on the right side Y-axis.

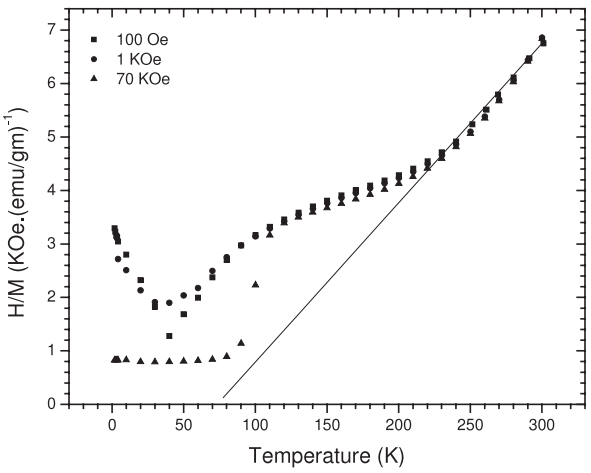

Figure 7. Inverse susceptibility (H/M) versus temperature curves for $Sm_{0.50}(Sr_{0.50}Ca_{0.50})_{0.50}MnO_3$; the solid line shows the linear fitting for 100 Oe data.

decrease in M at 40 K is not as evident for the highest field (70 kOe) data.

It is noticeable quite significantly that at low temperatures there is a very abrupt and marked increase in the moment between the fields of 10 and 70 kOe, namely, from 0.2 to 3.2 μ_B/Mn. This is suggestive of a field dependent transition from the AFM to FM phase. It may also be described as the melting of the AFM phase on the application of a high enough field, converting a large fraction of AFM phase into the FM one. This point will be further discussed in the magnetization versus field measurements.

The very strong decrease in the FM phase observed in this system (where Ca partially substitutes for Sr), particularly for low applied fields, originates from the smaller average cationic size $\langle r_A \rangle$ for the Ca doped composition as compared to that for Sr. As the mean cationic size on the A sublattice, $\langle r_A \rangle$, decreases, the distortion in MnO_6 octahedra increases, which in turn generates a smaller bandwidth W and in general reduces the double exchange interaction responsible for the ferromagnetic alignments.

3.2. Field dependence of DC magnetization

The development of different magnetic phases can be seen with reference to the magnetization behaviour as a function of field (M versus H). Hence, to get more insight into the spin structure, magnetization was also recorded as a function of field at different temperatures. All the $M(H)$ loops discussed here were recorded in zero field cooled mode.

Figure 8 shows $M(H)$ loops for undoped $Sm_{0.50}Sr_{0.50}MnO_3$ composition taken at three different temperatures, 4, 40 and 180 K. These particular temperatures were chosen with reference to the observations already made in the context of the $M(T)$ measurements.

At 4 K (figure 8(a)), the system is initially (segment 1 in figure) a mixture of FM and AFM phases. With the increase of the field there is a rapid rise corresponding to the alignment of the ferromagnetic part ($H < 10$ kOe), while from 10 to 30 kOe there is an almost linear increase in the magnetization giving the contribution of the AFM phase. At $H_{dc} = 30$ kOe the melting of the AFM is suggested by the abrupt jump in magnetization. On reversing the field (curve (2)) there is a large high field hysteresis due to the melted CO–AFM state. The irreversible nature of the transition from AFM to FM is evident since the AFM phase is not fully recovered on lowering the field. However, the melting of the AFM phase in curve (1) does not completely eliminate the AFM phase and some indication of melting is still to be seen in curve (3) at $H \sim 32$ kOe.

At $T \sim 40$ K (figure 8(b)), the temperature where this sample displayed a maximum in the magnetization data ($M(T)$), the indication of melting is still evident ($H_M = 22$ kOe) but the degree of irreversibility between the first and last loops (curves (1) and (3)) is smaller as compared to the $T \sim 4$ K loop. This latter feature is understood to be due to the lower AFM fraction at this temperature as compared to $T \sim 4$ K. The maximum magnetization obtained in this composition is 2.7 μ_B/Mn, which is significantly less than the saturation moment of 3.5 μ_B/Mn expected in the 50–50 CMR manganites.

At $T = 180$ K (figure 8(c)) the system is obviously in an AFM state, as evidenced by the very small and linear $M(H)$ response. There is a very distinct rise in the magnetization

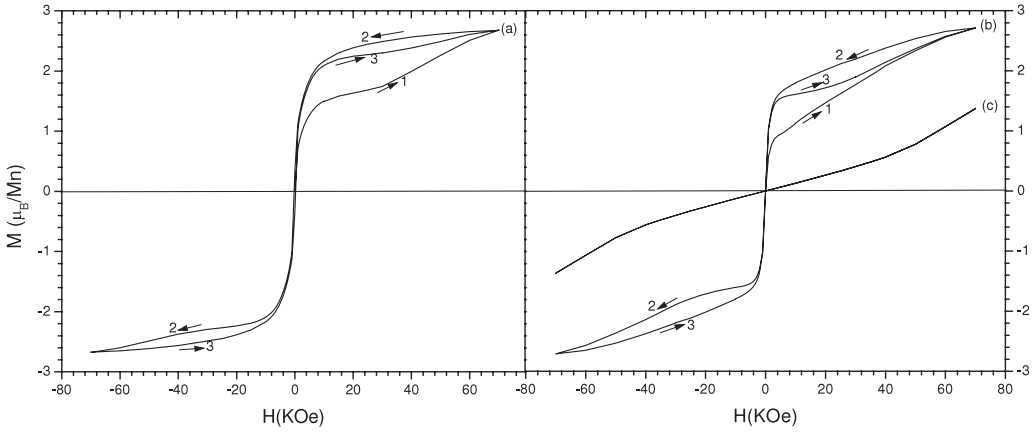

Figure 8. $M(H)$ loops for $Sm_{0.50}Sr_{0.50}MnO_3$ recorded at three different temperatures: (a) 4 K, (b) 40 K, (c) = 180 K.

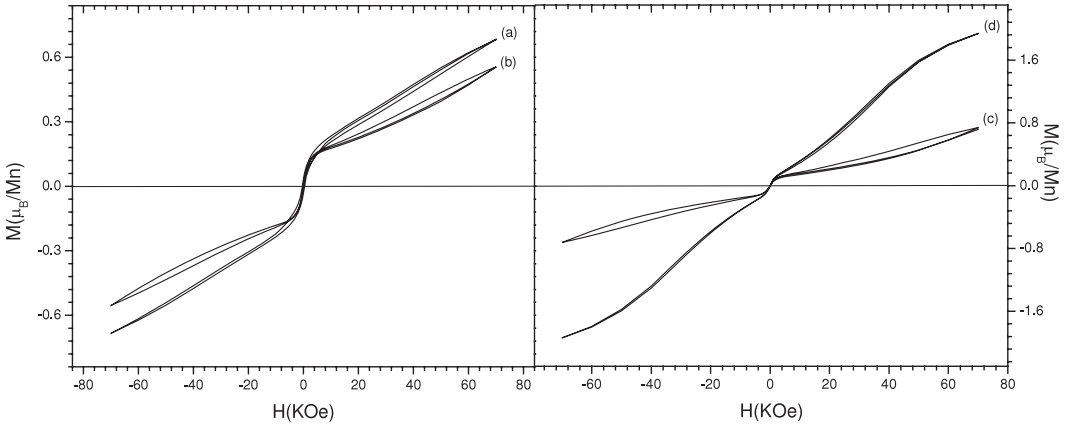

Figure 9. $M(H)$ loops for $(Nd_{0.50}Sm_{0.50})_{0.50}Sr_{0.50}MnO_3$ recorded at four different temperatures: (a) 4 K, (b) 40 K, (c) 110 K, (d) 190 K. (a) and (b) are on the left Y-axis while (c) and (d) are on the right Y-axis.

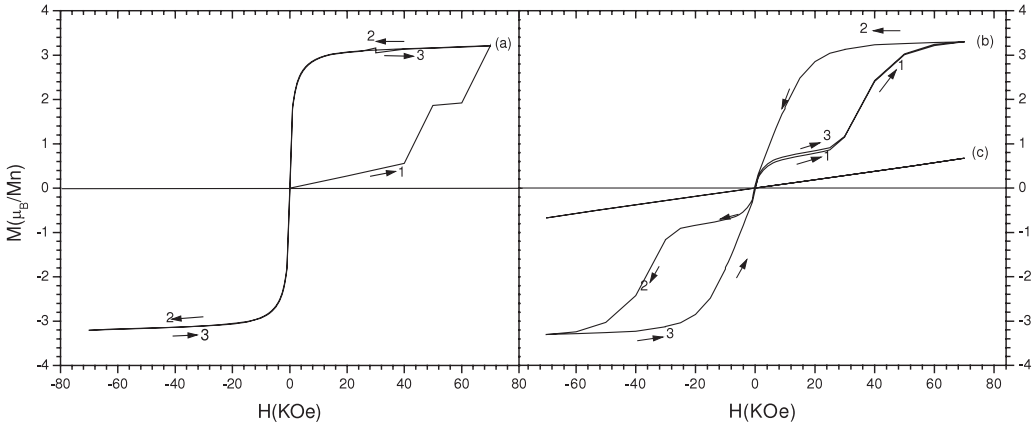

Figure 10. $M(H)$ loops measured at three different temperatures for $Sm_{0.50}(Sr_{0.50}Ca_{0.50})_{0.50}MnO_3$: (a) 4 K, (b) 40 K, (c) 180 K.

at $H \sim 43$ kOe, suggesting the melting of at least a portion of the AFM phase. It is noticeable that at this temperature the melting is a completely reversible effect, unlike the cases discussed for lower temperatures. Apparently the CO–AFM phase is highly stable at this temperature and the transitions are thermodynamically reversible.

Figure 9 shows the $M(H)$ loops for $(Nd_{0.50}Sm_{0.50})_{0.50}Sr_{0.50}MnO_3$ composition at four different temperatures, 4, 40, 110 and 190 K. These particular temperatures were chosen with reference to the observations already made in the context of the $M(T)$ measurements of this particular composition.

The hysteresis loops demonstrate the presence of two stable phases with no evidence of melting. At low fields a sharp rise is due to the presence of the ferromagnetic phase, while later a continuous linear rise can be attributed to the presence of the AFM phase. This particular composition shows a maximum magnetization value of 2 μ_B/Mn for $T =$ 190 K, significantly less than the maximum magnetization observed for the undoped composition (2.7 μ_B/Mn). It appears that the AFM fraction has *increased* for the Nd doped system as compared to the undoped composition. The reason for the presence of this large AFM part for $(Nd_{0.50}Sm_{0.50})_{0.50}Sr_{0.50}MnO_3$ composition is due to the *decrease of size mismatch between cations* on the substitution of 50% Nd in place of Sm. Although the average cationic size $\langle r_A \rangle$ has increased from 1.221 to 1.228 Å with the substitution of Nd, an effect that tends to stabilize the DE interaction, at the same time the mismatch factor σ^2 decreases from 7.92×10^{-3} to 6.84×10^{-3} Å^2. This latter change, on the other hand, supports the charge ordering phenomenon, leading to lower magnetization value [6].

$M(H)$ loops for the Ca doped composition $Sm_{0.50}(Sr_{0.50}Ca_{0.50})_{0.50}MnO_3$ at 4, 40 and 180 K are shown below in figure 10. The unusual and highly irreversible nature of the magnetization response is evident for the lowest temperature, $T \sim 4$ K. In curve (1), the virgin system shows a linear increase of magnetization with applied fields up to 40 kOe, which indicates that the system is purely in AFM state. At 40 kOe, there is a very abrupt jump in the magnetization, indicating the melting of a significant fraction of the AFM lattice between 40 and 50 kOe. From $H =$ 50–60 kOe the moment appears to be almost constant. This is followed by another sharp jump at 60 kOe, which shows the melting of a large fraction of the remaining AFM component, and the magnetization attains the maximum value of 3.2 μ_B/Mn at 70 kOe applied field (close to the maximum expected value of 3.5 μ_B/Mn). The melting of the AFM state at this temperature is completely irreversible and the system shows a typical ferromagnetic-like

behaviour in the remaining field cycles (curves (2) and (3) of figure 10(a)). Hence it appear that the AFM state appearing in this Ca doped composition melts completely and irreversibly, and almost full FM alignment is obtained at the higher fields ($H > 60$ kOe). This is different from the behaviour discussed above for the undoped and Nd doped composition. The basis of these differences will be discussed later in terms of the different types of AFM phases that are expected in these different compositions on the basis of the different average sizes.

At $T = 40$ K, the hysteresis loop for the Ca doped composition shows a rapid rise in the moment at low fields due to the presence of FM component at this temperature. This is followed by a slow linear growth of magnetization indicating the presence of the large amount of the AFM phase. At $H_{dc} = 26$ kOe, a large fraction of this AFM lattice is melted and the moment rises sharply and attains the maximum value of 3.3 μ_B/Mn. The melting of the AFM phase observed here is almost completely reversible with field, as evidenced from traces (2) and (3) of figure 10(b). This is to be contrasted to the situation at 4 K. If the irreversible nature of the melting transition at lower temperature is to be attributed to the fact that the system gets trapped in the FM state at high fields and is separated from the AFM state by an energy barrier that it cannot cross due to the low thermal energy available, then at 40 K these barriers are sufficiently small and the thermal energy is sufficient for the spins to cross these barriers with field increase. This removes the history dependence of the system.

At $T \sim 180$ K (figure 10(c)) the loop is observed to be typical of an AFM. The value of the moment is very small suggesting that the system is in a fully AFM state, with no trace of FM or of a melting transition. This is in accordance with the results observed in the $M(T)$ data, which indicate that between 230 and 110 K this composition consists of an AFM phase along with some PM component.

3.3. Resistivity measurements

The resistivity of the system was measured in the usual four probe configuration with a measuring current of up to 100 microamperes. Figure 11 shows the variation of resistivity with the temperature for the Sm–Sr composition. The system initially displays insulating behaviour for $T > 30$ K and the resistivity peaks at $T \sim 30$ K, below which temperature metallic behaviour is evident.

Cooling down from room temperature a sharp rise in $\rho(T)$ is observed at $T \sim 200$ K. This rise in resistivity corresponds to the emergence of the AFM correlations within the primarily PM phase, as observed in the magnetization measurements. Although the magnetic measurements have shown the presence of ferromagnetic correlation between 130 and 40 K, the resistivity remains insulating in this temperature range and does not show metallic behaviour, which is generally accompanied by double exchange mediated ferromagnetism in these perovskite materials. This overall insulating behaviour is due to the presence of a large fraction of the AFM phase along with the FM phase, as evident from small values of moment and the metamagnetic

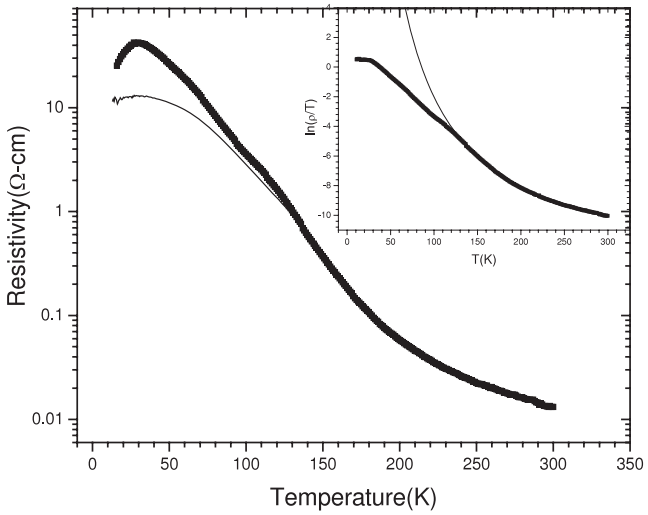

Figure 11. Temperature dependence of resistivity for $Sm_{0.50}Sr_{0.50}MnO_3$; the solid line in the main figure shows the data taken in 6 kOe applied field; the inset shows the fitting using the polaronic model as described by equation (1) in the text.

transitions observed in magnetic measurements. Recent neutron diffraction and resistivity measurements made on $Sm_{0.50}Sr_{0.50}MnO_3$ composition [14] have also shown that the relative fraction of the AFM phase with insulating character increases with decreasing temperature down to 50 K, hence it presumably does not allow the development of a percolating path for the FM metallic phase. According to the authors of [14], an insulator–metallic transition occurs at a particular temperature with the completion of the phase separation where the FM phase forms a conductive path. In their data this occurs at 50 K, while in our case the system develops a percolating conducting path below 30 K.

Resistivity data were also recorded in the presence of a 6 kOe applied DC field and the decrease in resistance is apparent in the data shown with a solid line in figure 11. It was found that percentage magnetoresistance (%MR), defined as $\%MR = \frac{\rho_0 - \rho_H}{\rho_0} \times 100$, where ρ_0 is the resistivity in the absence of the applied field while ρ_H is the value in the presence of the applied field, has the value of ∼66% for this particular composition at $T = T_p$ (30 K).

High temperature resistivity data was analysed using the small polaronic [18] and variable range hopping models [19]. However, only the small polaronic model, i.e.

$$\ln \frac{\rho}{T} = \ln A + \frac{W}{k_B T} \tag{1}$$

was able to fit the data meaningfully down to 130 K. In equation (1) W is the activation energy while A is a constant. The activation energy for the system hence determined was 104 meV. In the lower temperature range 130–30 K, $\rho(T)$ continues increasing but the observed values lie well below those predicted by extending the high temperature polaronic fit to the data.

The temperature dependence of resistivity for $(Nd_{0.50}Sm_{0.50})_{0.50}Sr_{0.50}MnO_3$ composition is shown in figure 12. The behaviour of the system is insulating over the entire

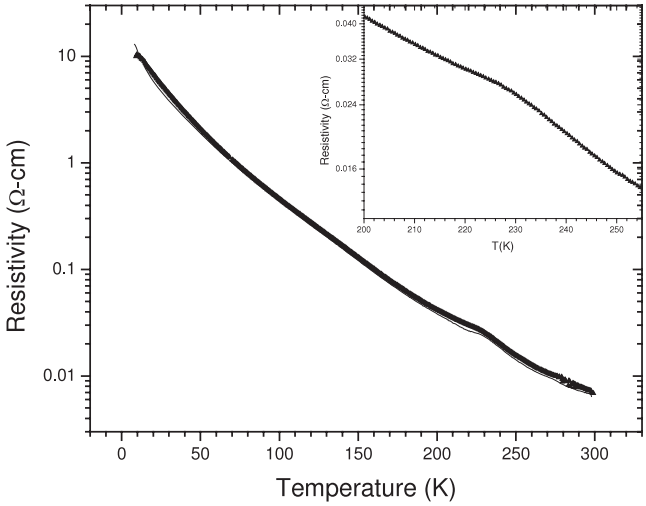

Figure 12. Temperature dependence of resistivity for the $(Nd_{0.50}Sm_{0.50})_{0.50}Sr_{0.50}MnO_3$ composition. The solid line shows the data recorded at 6 kOe applied dc field. The inset shows the resistivity data from 200 to 255 K on an expanded scale.

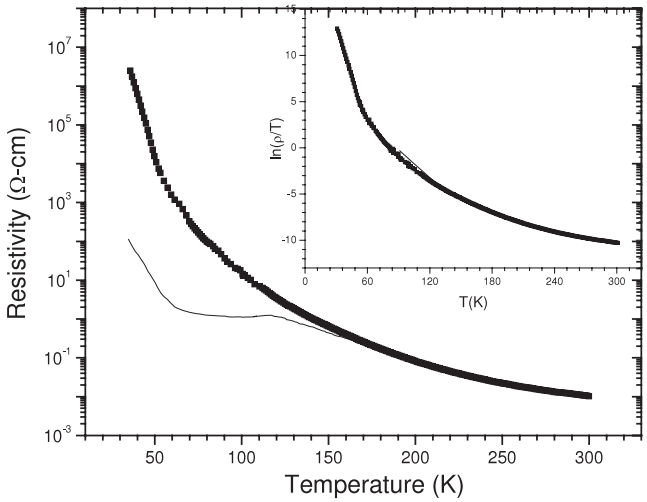

Figure 13. Temperature dependence of resistivity for $Sm_{0.50}(Sr_{0.50}Ca_{0.50})_{0.50}MnO_3$; the solid line shows the data taken in 6 kOe applied field; the inset shows the fitting using the polaronic model as described in the text by equation (1).

temperature range 10 K $< T <$ 300 K. Compared to the undoped composition the overall values of resistivity were seen to be decreased but no metal–insulator transition was observed. The $\rho(T)$ curve for $(Nd_{0.50}Sm_{0.50})_{0.50}Sr_{0.50}MnO_3$ composition shows only a small bump or change of slope at $T \sim 230$ K, which is shown on an expanded scale in the inset of figure 12. It can also be seen from the main figure that the application of a 6 kOe DC field did not produce any major decrease in the resistivity at any temperature. The maximum field induced decrease was only ∼10% and was observed at $T = 220$ K. Hence the AFM state observed for the $(Nd_{0.50}Sm_{0.50})_{0.50}Sr_{0.50}MnO_3$ composition can be regarded as being more stable in the presence of an applied magnetic field as compared to the undoped composition. These observations suggest that while the substitution of 50% Nd in place of Sm in the $Sm_{0.50}Sr_{0.50}MnO_3$ composition may have caused the increase of the one electron band width, thus increasing the itinerancy of the Mn e_g electrons, this delocalization is still confined to isolated FM domains. The insulating AFM phase, which is coexistent with these conducting domains, does not allow the charge carriers to delocalize completely and the system does not become metallic down to 10 K.

The insulating characteristics are further enhanced by the addition of Ca to the $Sm_{0.50}Sr_{0.50}MnO_3$ composition. Figure 13 illustrates this behaviour, where not only is the metal–insulator transition is completely eliminated but a very steep rise in the resistivity is observed. The very large values of the resistivity, approaching 10^7 Ω cm at the lowest temperatures, are in sharp contrast to those observed in the undoped and Nd doped systems and indeed compare well to the values typical for charge ordered perovskites. It was also noticeable that these large values of resistivity were significantly reduced on the application of a modest field of 6 kOe (solid line in figure 13). Interestingly, in the range 60 K $< T <$ 120 K the resistivity in field is seen to be almost constant. This coincides with the temperature region where the ferromagnetic upturn is clearly visible in the $M(T)$ data at moderate fields (figures 5(a) and (b)). Below this temperature range the very rapid rise in the resistivity coincides with the antiferromagnetic transition apparent in the same figures, 6(a) and (b). Taken together, the zero field and field dependent resistivity data suggest that between 120 and 60 K the application of a moderately high field is sufficient to prevent the development of the CO–AFM state. The CO–AFM melts on the application of the field and the resistive rise is suppressed till ∼60 K. The percentage change in the resistance coefficient as defined above was seen to be ∼99.9% at 40 K.

High temperature data for this composition were analysed using the polaronic model (equation (1)) and were found to fit the data well for $T > 130$ K. The fit is shown in the inset of figure 13. The activation energy obtained from the fit was determined to be 120 meV and is seen to be larger than that obtained for the undoped composition (104 meV).

3.4. Thermoelectric power (TEP) measurements

Figure 14 shows the TEP data for the $Sm_{0.50}Sr_{0.50}MnO_3$ and $(Nd_{0.50}Sm_{0.50})_{0.50}Sr_{0.50}MnO_3$ compositions. Due to experimental limitations, we were not able to measure the thermopower for the $Sm_{0.50}(Sr_{0.50}Ca_{0.50})_{0.50}MnO_3$ composition, presumably due to the very high values of resistivity, that tended to lead to instabilities in the TEP voltages. All the data discussed here were recorded during heating of the sample from 80 K to room temperature. We shall discuss the variations of the thermoelectric power in the light of the observations and conclusions drawn from the magnetization and resistivity data. For the undoped composition, $Sm_{0.50}Sr_{0.50}MnO_3$, the thermoelectric power (figures 14(a)) starts out at $S \sim -25\ \mu V\ K^{-1}$ for $T = 298$ K and with decreasing temperature its absolute value decreases to $T \sim 240$ K. Below 230 K the absolute value of S rises sharply with further decrease of temperature. The origin of this sharp rise is the formation of AFM domains

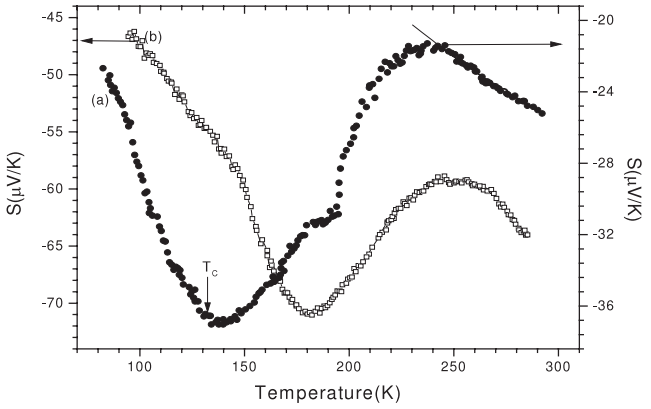

Figure 14. Thermopower as function of temperature: (a) $Sm_{0.50}Sr_{0.50}MnO_3$ (shown on the right side Y-axis), (b) $(Nd_{0.50}Sm_{0.50})_{0.50}Sr_{0.50}MnO_3$ (shown on the left side Y-axis); the solid line shows the fitting of the polaronic model (equation (2)) for the undoped composition.

within the PM matrix as observed in the magnetic data of this particular composition. Coexistence of these magnetically ordered (AFM) and disordered (paramagnetic) phases increases the spin entropy carried by charge carriers, which is reflected as an increase in the absolute value of the TEP. On further lowering the temperature, a sharp decrease of absolute value of TEP is observed for $T < 130$ K. As the magnetization measurements (figure 2) show, ferromagnetic alignment in the bulk is initiated at this temperature and appears to be responsible for the decrease of magnetic scattering. We attribute the decrease in S to a purely magnetic origin, since the resistivity data show the metallic transition occurring at a much lower temperature ($T \sim 30$ K).

As in the resistivity data, the high temperature TEP data ($T > 240$ K) were also analysed using the polaronic transport model. The general form of the polaronic contribution to the Seebeck coefficient is given as [20]

$$S_c = (k_B/e)((\varepsilon_a/k_B T) + \alpha). \quad (2)$$

Here ε_a is the activation energy while α is a constant. A value $\alpha < 1$ is understood to indicate the hopping due to small polarons while $\alpha > 2$ suggests the existence of large polarons [21].

The solid line shown in figure 14 gives the fitting of equation (2) for the undoped composition. The activation energy calculated from this fitting turns out to be 5.6 meV, which is significantly lower than that obtained from the resistivity data. This difference in activation energies obtained from TEP and resistivity measurements is commonly seen in polaronic systems and further illustrates that charge transport is dominated by thermally activated polarons [20]. The value of α calculated from the fit using equations (2) is -0.51 ± 0.01 and is in good agreement with that obtained by Banerjee *et al* [22] and Bhattacharya *et al* [23] on another 50–50 composition. The value of α as determined by us supports the small polaron hopping as the dominant conduction mechanism in this regime of temperature.

The $S(T)$ curve for $(Nd_{0.50}Sm_{0.50})_{0.50}Sr_{0.50}MnO_3$ composition is shown in figure 14(b). The qualitative behaviour is similar to that of the undoped sample; however, the absolute value of the TEP has increased significantly. At high temperatures ($T > 265$ K), where the system is in the PM phase, the TEP shows polaronic behaviour like the undoped composition in a similar phase. From 265 to 240 K the TEP was almost constant, while for $T < 240$ K S rises sharply, peaks at its maximum negative value at $T \sim 180$ K and thereafter decreases to the lowest temperature. However, this decrease in $S(T)$ shows a distinct slowing down for $T < 150$ K.

The magnetic data for the $(Nd_{0.50}Sm_{0.50})_{0.50}Sr_{0.50}MnO_3$ composition have shown the emergence of ferromagnetic correlations in the vicinity of 240 K. But this temperature cannot be considered as representing the ferromagnetic phase over the whole sample, since these correlations are only on a very small length scale and the ferromagnetism appears only in the form of small clusters. The competition between the two phases (magnetically ordered and disordered) enhances the spin scattering and the effect is reflected in the increase of the TEP values in the vicinity of 240 K. However, as evidenced from the sharp decrease of the moment in the magnetization measurements, below 200 K this two phase system is dominated by the AFM phase. As $S(T)$ is sensitive to the (spin) entropy carried by the charge carriers, any ordered arrangement (FM or AFM) causes the reduction of TEP values. Hence the decrease in the TEP at $T \sim 180$ K is indicative of the stabilization of AFM phase as opposed to the two-phase system at higher temperatures. A similar decrease in S has been reported in the $Sm_{0.45}Sr_{0.55}MnO_3$ system in the AFM state [24]. Hejtmanek *et al* [25] have also shown the decrease in TEP values for pure AFM systems at PM to AFM transition temperatures.

For this same system the change in the slope in $S(T)$ data observed at still lower temperatures, $T < 150$ K (figure 14(b)), can also be correlated with the increase of spin entropy around this temperature. As the M(T) data have shown, at these low temperatures there is *again* a growth of FM correlations alongside the dominant AFM phase. This growth of FM correlations within the AFM phase again leads to the enhancement of the spin disorder and the sharp decrease in $S(T)$ slows down at 150 K.

4. Discussion

We have observed that in the $Sm_{0.50}Sr_{0.50}MnO_3$ system, which lies close to the boundary separating the FM and CO–AFM phases, the two phases coexist or dominate one another depending on temperature and field. The parent composition has shown the emergence at $T \sim 230$ K of AFM correlations embedded within the PM phase. Below 130 K this system shows the development of an FM phase but the values of magnetic moment and the metamagnetic transition observed in the hysteresis loops suggest the presence of an AFM phase as well and the system remains in the two phase state down to the lowest temperature measured (10 K). Metallic behaviour in this particular system was however only observed below 30 K. The thermoelectric power (TEP) exhibits a sharp decrease with the onset of FM correlations ($T < 130$ K). The inconsistency

between the trends exhibited by the resistive and the TEP behaviour, with the former exhibiting metallicity only below 30 K while the TEP shows a sharp decrease below 130 K, can be interpreted in the light of the neutron diffraction study carried out by Kurbakov *et al* [14]. This latter study has shown a continuous increase of the volume fraction of the AFM phase within the temperature range 50–135 K. According to the authors [14], this phase begins to form in the vicinity of grain boundaries, preventing metallization of inter-grain contacts. We understand that as the thermopower is significantly less affected by grain boundaries the improved heat flow *within* the grains, occurring as a consequence of the FM correlations, leads to a rapid decrease in the thermoelectric power values. Furthermore, the moderately high resistivity values observed in the undoped $Sm_{0.50}Sr_{0.50}MnO_3$ composition suggest that the charge ordering is not of purely CE type, which is generally accompanied by very large values of resistivity (10^{5-6} Ω cm). It seems that the charge ordering appearing in this system may be arising from a combination of A-type and CE-type orbital ordering, the former being characterized by rather low resistivity within the FM layers. Neutron diffraction on similar systems has shown that the AFM phase appearing in the $Sm_{0.50}Sr_{0.50}MnO_3$ system is of the A type [14]. In the A-type AFM state the e_g electrons supposedly occupy the two-dimensional $d_{x^2-y^2}$ orbitals [26] rather than the one-dimensional $d_{3z^2-r^2}$. In the heavily doped region, the e_g electron system gains the maximum kinetic energy (at the cost of lattice energy) when the $d_{x^2-y^2}$ orbitals form a pseudo-2D band, and if such a pseudo-2D band were realized the in-plane exchange interaction would be ferromagnetic, mediated by the itinerant $d_{x^2-y^2}$ electrons, while antiferromagnetic interaction should dominate along the z-direction [27]. A similar A-type AFM state is also observed for other half doped systems, e.g. for $Pr_{0.50}Sr_{0.50}MnO_3$ [28, 29] and for $(La_{0.50}Nd_{0.50})_{0.50}Sr_{0.50}MnO_3$ [30].

Substitution of 50% Nd in place of Sm in the undoped $Sm_{0.50}Sr_{0.50}MnO_3$ composition increased the average cationic radius $\langle r_A \rangle$ from 1.21 to 1.23 Å, thereby strengthening the double exchange (DE) mechanism and increasing the ferromagnetic transition temperature. Our magnetic data show that, although the ferromagnetic transition temperature has increased for the $(Nd_{0.50}Sm_{0.50})_{0.50}Sr_{0.50}MnO_3$ composition as compared to the undoped case, at the same time the AFM phase appearing in this composition has also become stronger and remains dominant for $T < 180$ K even at a 70 kOe applied field. This effect can be explained by the appreciable decrease in the mismatch factor (σ^2) for $(Nd_{0.50}Sm_{0.50})_{0.50}Sr_{0.50}MnO_3$ system as compared to the undoped composition. Addition of Nd has decreased σ^2 from 7.92×10^{-3} Å^2 (for the undoped composition) to 6.84×10^{-3} Å^2 (for the $(Nd_{0.50}Sm_{0.50})_{0.50}Sr_{0.50}MnO_3$ composition). In this phase separated system the decrease of the mismatch factor between the cations supports the magnetic interactions (whether FM or AFM) present in the respective microdomains [6]. Hence, although the ferromagnetic transition temperature has been raised to 220 K for this composition, at the same time the coupling within the AFM domains has become stronger and the metamagnetic transitions which were clear for undoped composition are absent here for Nd doped composition. Due to this strong effect of σ^2 on both FM and AFM phases, the two phase nature for the $(Nd_{0.50}Sm_{0.50})_{0.50}Sr_{0.50}MnO_3$ system has also increased, which we understand to be the main source of the observed increase of thermopower.

The partial replacement of Sr with smaller size Ca ions in the $Sm_{0.50}Sr_{0.50}MnO_3$ composition causes an appreciable decrease of average cation size from 1.21 to 1.18 Å, that in turn leads to an appreciable decrease of the lattice constants. This substitution appears to narrow the one electron bandwidth (W), leading to strong localization of the e_g electron in $Sm_{0.50}(Sr_{0.50}Ca_{0.50})_{0.50}MnO_3$ composition. With the decrease of W, the double exchange is almost eliminated, leaving the system in the purely AFM state. Furthermore, the AFM state appearing in the Ca substituted composition is accompanied by very high values of resistivity. This behaviour of resistivity suggests that reduction of W has suppressed the A-type AFM ordering and the CE-type charge ordering is realized in the crystal. In CE-type charge ordering e_g electrons occupy the $d_{3z^2-r^2}$ orbitals, accompanied by large Jahn–Teller distortion of the MnO_6 octahedra, leading to the strong localization of charge carriers.

5. Conclusion

In conclusion, we have shown that in a system with a comparatively wide one electron bandwidth, with a composition close to the FM/AFM–CO boundary, i.e. $Sm_{0.50}Sr_{0.50}MnO_3$, the change of one electron bandwidth due to suitable dopants has drastic effects on the two phase nature of the system. As the bandwidth increases (for the $(Nd_{0.50}Sm_{0.50})_{0.50}Sr_{0.50}MnO_3$ composition) the phase coexistence of FM and AFM increases. This increase of the two phase nature of the system is due to the decrease of the mismatch factor between cations. On the other hand, as the bandwidth decreases (for the $Sm_{0.50}(Sr_{0.50}Ca_{0.50})_{0.50}MnO_3$ composition) the system transforms from a mixture of FM and AFM phases to a purely AFM and charge ordered one. At the same time there are indications that the AFM phase present transforms from a mixture of A-type and CE-type orbital ordering to a purely CE-type orbital ordering that is accompanied by very high values of resistivity.

References

[1] Goodenough J B 1955 *Phys. Rev.* **100** 564
[2] de Gennes P-G 1960 *Phys. Rev.* **118** 141
[3] Damay F, Martin C, Maignan A and Raveau B 1997 *J. Appl. Phys.* **82** 6181
[4] Barnabe A, Hervieu M, Martin C, Maignan A and Raveau B 1998 *J. Appl. Phys.* **84** 5506
[5] Tomioka Y, Okimoto Y, Jung J H, Kumai R and Tokura Y 2003 *Phys. Rev.* B. **68** 094417
[6] Rodriguez-Martinez L M and Attfield J P 1996 *Phys. Rev.* B **54** R15622
[7] Motome Y, Furukawa N and Nagaosa N 2003 *Phys. Rev. Lett.* **91** 167204
[8] Sundaresan A, Maignan A and Raveau B 1997 *Phys. Rev.* B **56** 5092
[9] Wang Y Q, Ian Maclaren and Duan X F 2001 *J. Appl. Phys.* **90** 488
[10] Martin C, Maignan A, Hervieu M and Raveau B 1999 *Phys. Rev.* B **60** 12191

[11] Ivanov V Y, Mukhin A A, Travkin V D, Prokhorov A S and Balbashov A M 2003 *J. Mag. Magn. Mater.* **258–259** 535
[12] Tomioka Y, Kuwahara H, Asamitsu A, Kasai M and Tokura Y 1997 *Appl. Phys. Lett.* **70** 3609
[13] Shames A I, Yakubovsky A, Amelichev V, Gorbenko O and Kaul A 2002 *Solid State Commun.* **121** 103
[14] Kurbakov A I, Lazuta A V, Ryzhov V A, Trounov V A, Larionov I I, Martin B, Maignan A and Hervieu M 2005 *Phys. Rev.* B **72** 184432
[15] Kuwahara H, Moritomo Y, Tomioka Y, Asamitsu A, Kasai M, Kumai R and Tokura Y 1997 *Phys. Rev.* B **56** 9386
[16] Aslam A, Hasanain S K, Zubair M, Akhtar M J and Nadeem M 2002 *J. Phys.: Condens. Matter* **14** 10305
[17] Damay F, Nguyen N, Maignan A, Hervieu M and Raveau B 1996 *Solid State Commun.* **98** 997
[18] Snyder G J, Hiskes R, Dicarolis S, Beasley M R and Geballe T H 1996 *Phys. Rev.* B **53** 14434
[19] Viret M, Ranno L and Coey J M D 1997 *Phys. Rev.* B **55** 8067
[20] Mott N F and Davis E A 1979 *Electronics Process in Non Crystalline Materials* (Oxford: Clarendon)
[21] Sega K, Kuroda Y and Sakata H 1998 *J. Mater. Sci.* **33** 1303
[22] Banerjee A, Pal S, Bhattacharya S and Chaudhuri B K 2001 *Phys. Rev.* B **64** 104428
[23] Bhattacharya S, Banerjee A, Pal S, Mukherjee R K and Chaudhuri B K 2003 *J. Appl. Phys.* **93** 356
[24] Maignan A, Martin C, Hervieu M and Raveau B 2001 *J. Appl. Phys.* **89** 2232
[25] Hejtmanek J, Jirak Z, Pollert E, Sedmidubsky D and Strejc A 2002 *J. Appl. Phys.* **91** 8275
[26] Hirota K, Moritomo Y, Fujioka H, Kubota M, Yoshizawa H and Endoh Y 1998 *J. Phys. Soc. Japan* **67** 3380
[27] Moritomo Y, Akimoto T, Nakamura A, Ohoyama K and Ohashi M 1998 *Phys. Rev.* B **58** 5544
[28] Tomioka Y, Asamitsu A, Moritomo Y, Kuwahara H and Tokura Y 1995 *Phys. Rev. Lett.* **74** 5108
[29] Kawano H, Kajimoto R, Yoshizawa H, Tomioka Y, Kuwahara H and Tokura Y 1997 *Phys. Rev. Lett.* **78** 4253
[30] Moritomo Y, Kuwahara H, Tomioka Y and Tokura Y 1997 *Phy. Rev.* B **55** 7549